Optical Manipulation of a Magnon-Photon Hybrid System

C. Braggio,[1,*] G. Carugno,[1] M. Guarise,[1] A. Ortolan,[2,†] and G. Ruoso[2]
[1]*Dip. di Fisica e Astronomia and INFN, Sez di Padova, Via F. Marzolo 8, I-35131 Padova, Italy*
[2]*INFN, Laboratori Nazionali di Legnaro, Viale dell'Università 2, I-35020 Legnaro, Italy*
(Received 17 August 2016; published 8 March 2017)

We demonstrate an all-optical method for manipulating the magnetization in a 1-mm yttrium-iron-garnet (YIG) sphere placed in a ∼0.17 T uniform magnetic field. A harmonic of the frequency comb delivered by a multi-GHz infrared laser source is tuned to the Larmor frequency of the YIG sphere to drive magnetization oscillations, which in turn give rise to a radiation field used to thoroughly investigate the phenomenon. The radiation damping issue that occurs at high frequency and in the presence of highly magnetizated materials has been overcome by exploiting the magnon-photon strong coupling regime in microwave cavities. Our findings demonstrate an effective technique for ultrafast control of the magnetization vector in optomagnetic materials via polarization rotation and intensity modulation of an incident laser beam. We eventually get a second-order susceptibility value of $\sim 10^{-7}$ cm^2/MW for single crystal YIG.

DOI: 10.1103/PhysRevLett.118.107205

Introduction.—Nonthermal control of spins by short laser pulses is one of the preferable means to achieve ultrafast control of the magnetization in magnetic materials (see [1], and references therein), representing a breakthrough in potential applications ranging from high density magnetic data storage [2], spintronics [3], to quantum information processing [4,5]. Raman-type nonlinear optical processes have been exploited to excite coherent magnons in orthoferrites and garnets via high-intensity, subpicosecond pulses. For instance, in the weak ferromagnet dysprosium orthoferrite ($DyFeO_3$) the excitation of spin precession was observed with circularly polarized femtosecond laser pulses, shown to act as transient magnetic field pulses with estimated amplitude of the order of 1 T [6]. This phenomenon is referred to as inverse Faraday effect, and the induced magnetic field is directed along the wave vector of light. Magnetization oscillations have been excited by both linearly and circularly polarized laser pulses [7] in the weak ferromagnet iron borate ($FeBO_3$) through the impulsive stimulated Raman scattering. The efficiency of these processes is related to the mutual orientation of the magnetic and crystallographic axes and the light propagation direction. Vector control of the magnetization was also demonstrated in an antiferromagnetic crystal (NiO) by varying the delay between pairs of polarization-twisted ultrashort optical pulses [8].

In this work we introduce a new approach in optomagnetism based on multigigahertz repetition rate lasers with optical carrier f_0 [9]. The power spectrum of such mode-locked laser sources, as detected by ultrafast photodiodes, is a frequency comb that consists of several harmonics nf_r, where f_r is the repetition rate and n is a small number. Their Gaussian envelope is determined by the optical pulse temporal profile [10]. For example, our 4.6 GHz passively mode-locked oscillator delivers ∼10 ps-duration pulses that give rise to a frequency comb up to 100 GHz, and the first three harmonics have approximately the same amplitude. In principle, any harmonic of the comb can coherently drive the magnetization in the steady state through the process described in the present work, provided it is tuned to electron spin resonances of the magnetized material.

We study the spin dynamics in a hybridized system that consists of two strongly coupled oscillators, i.e., a microwave cavity mode and a magnetostatic mode related to ferromagnetic resonance (FMR) with uniform precession [11] of a single crystal yttrium-iron-garnet $Y_3Fe_5O_{12}$ sphere. Magnetic garnets [12,13] represent the ideal materials for such investigations for several reasons, including the possibility to realize large magneto-optical effects due to their strong spin-orbit coupling and intrinsically low magnetic damping [13–15].

We succeed to optically drive the precession of the spins electrodynamically coupled to the cavity photons with the first harmonic of the train of pulses at f_r tuned to one of the hybrid system's resonant frequencies. The process gives rise to a microwave field that is measured with a loop antenna critically coupled to the cavity mode. In this way, we have identified a new observable for the spin precession to explore optomagnetic phenomena. So far, experiments in this field have been performed with a magneto-optic pump-probe apparatus based on femtosecond lasers [1,8,13,16]. As it is well known, at very high values of frequency and magnetization, the energy radiated from oscillating magnetization through magnetic dipole radiation can be an issue for the dynamic control of the magnetization. For instance, in a polarized 1-mm yttrium-iron-garnet (YIG) sphere with linear susceptibility $\chi \sim 30$, the onset of

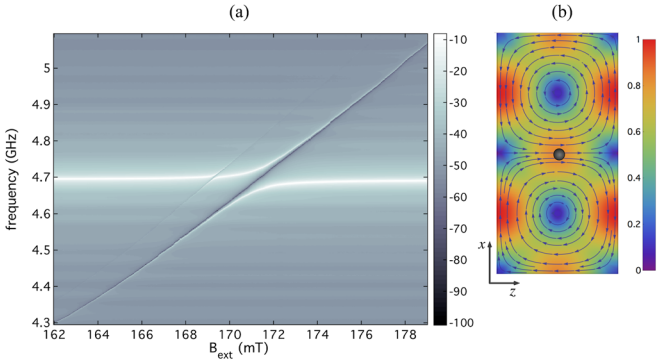

FIG. 1. Hybridizing magnons and microwave photons. (a) Cavity transmission spectrum measured as a function of the static magnetic field at room temperature. (b) Simulated magnetic-field distribution of the TE_{102} cavity mode. A static magnetic field B_{ext} is applied normal to the xz plane, and the microwave magnetic field at the YIG sphere (in black and not to scale in the representation) position is perpendicular to the static magnetic field. The color map represents the amplitude of the cavity magnetic field normalized to its maximum value.

radiation damping occurs at ~10 GHz [17]. However, the radiation damping mechanism can be conveniently suppressed in the microwave cavity-QED and strong coupling regimes [17,18], as we detail in the following for hybridized systems. Moreover, under remarkable conditions of hybridization, we get the control of relevant experimental parameters such as the number of spins, rf absorbed power, and the involved relaxation times. System hybridization is however not essential to observe the phenomenon described in the present work. In fact, we succeed in controlling the magnetization also in free space, but under experimental conditions that do not allow for accurate modeling.

Hybridized system characterization.—Strong interaction between light (i.e., photons stored in a cavity) and magnetized materials has been accomplished in several experiments that are paving the way toward the development of quantum information technologies [19–21]. Hybridization is commonly investigated by measuring the microwave-cavity transmission spectrum as a function of the static magnetic field, as summarized in Fig. 1 for our experimental setup, even though, very recently, some authors have reported electric detection via spin pumping [22]. A YIG sphere made by Ferrisphere Inc. with a radius of 1 mm is mounted at the center of a three-dimensional rectangular microwave cavity with dimensions $98 \times 42.5 \times 12.6\ \mathrm{mm}^3$. The cavity made of oxygen free copper has the TE_{102} mode frequency $\omega_c/2\pi \simeq 4.67$ GHz, and its internal cavity loss κ_{int}. This cavity has two ports characterized by the coupling coefficients κ_1 and κ_2 to the considered cavity mode. The sphere is glued to an alumina (aluminum-oxide) rod that identifies the crystal axis [110], perpendicular to the static magnetic field $\mathbf{B}_{\mathrm{ext}}$ (y axis) and parallel to the TE_{102} microwave magnetic field lines lying on the xz plane. Because of the strong coupling between the cavity mode and FMR mode an avoided crossing occurs when their resonant frequencies match. As derived in the input-output theory context [18,21], when the static magnetic field is tuned to drive the magnons in resonance with the cavity mode TE_{102}, the measured transmission coefficient can be written as

$$S_{21}(\omega) = \frac{\sqrt{\kappa_1\kappa_2}}{i(\omega-\omega_c) - \frac{\kappa_c}{2} + \frac{|g_m|^2}{i(\omega-\omega_{\mathrm{FMR}})-\gamma_m/2}}, \qquad (1)$$

where ω_{FMR} and γ_m are the frequency and linewidth of the FMR mode, $\kappa_c/2\pi = (\kappa_1+\kappa_2+\kappa_{\mathrm{int}})/2\pi$ is the total cavity linewidth, and g_m is the coupling strength of the FMR mode to the cavity mode. The latter parameter is proportional to the square root of the number of precessing spins N_s, i.e., $g_m = g_0\sqrt{N_s}$, where $g_0 = \gamma_e\sqrt{\mu_0\hbar\omega_c/V_c}$ is the coupling strength of a single spin to the cavity mode, with $\gamma_e = 2\pi \times 28$ GHz/T being the electron gyromagnetic ratio, μ_0 the permeability of vacuum, and V_c the cavity volume.

As discussed in the seminal paper of Bloembergen and Pound [17], the poles at the anticrossing point $\omega_{\mathrm{FMR}} = \omega_c \equiv \omega_0$ are given by

$$p_\pm = i(\omega_0 \pm \sqrt{|g_m|^2 - [(\kappa_c-\gamma_m)/4]^2}) - \frac{1}{2}\left(\frac{k_c}{2}+\frac{\gamma_m}{2}\right), \qquad (2)$$

and their imaginary and real parts represent the frequencies

$$\omega_\pm = \omega_0 \pm \sqrt{|g_m|^2 - [(\kappa_c-\gamma_m)/4]^2}$$

and the linewidths $\gamma_\pm = 1/2(k_c+\gamma_m)$ of the hybridized modes, respectively. From Eq. (2) hybridization clearly occurs only if $|g_m|^2 - [(\kappa_c+\gamma_m)/4]^2 > 0$ and, as a consequence, hybridized modes have the same decay time, independent of the sample or cavity volume and coupling strengths, i.e., $\bar{\tau} \equiv \tau_\pm = (2/\tau_c + 2/\tau_2)^{-1}$, where $\tau_c = 2/\kappa_c$ and τ_2 are the loaded cavity decay time and the spin-spin relaxation time, respectively. In the absence of hybridization, the term under the square root in Eq. (2) is negative and thus the poles have the same frequency ω_0, with two relaxation times τ_c and $\tau^* = (1/\tau_r + 1/\tau_2)^{-1}$ that correspond to the damping of the cavity mode and magnetization mode in the presence of radiation damping $\tau_r = \kappa_c/2/|g_m|^2$.

In our experimental apparatus for $B_{\mathrm{ext}} \simeq 0.17$ T we achieve a strong coupling regime with $g_m/2\pi = 57$ MHz; thus, the involved precessing spins are $N_s \sim 10^{20}$. Along with the mode frequencies $f_+ = 4.7247$ GHz and $f_- = 4.6677$ GHz, the fit of the measured S_{21} coefficient to Eq. (1) gives the mode decay times $\bar{\tau} \simeq 65$ ns of the hybridized system, compatible with the value of τ_2 provided by the manufacturer and the measured τ_c.

Photoinduced magnetization.—Once the hybrid system has been characterized, the experimental apparatus

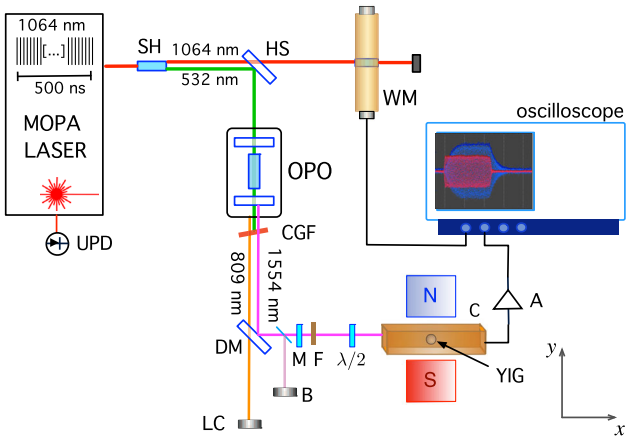

FIG. 2. Schematic representation of the experimental arrangement. The 1064 nm-wavelength macropulse delivered by a MOPA laser is frequency doubled (SH) to synchronously pump an optical parametric oscillator (OPO). The laser repetition rate, macropulse uniformity, and energy are monitored at an InGaAs ultrafast photodiode (UPD), a coaxial waveguide device (WM) [23], and a bolometer B, respectively. The 809 nm OPO output beam intensity profile is adjusted at a digital laser camera (LC). To make sure that only emission at 1550 nm impinges on the YIG sphere, several optical filters are inserted in the beam path. CGF is a 610 nm long pass colored glass filter, F transmits $\lambda > 1500$ nm, and M is a 1064 nm, high reflectivity dielectric mirror. The harmonic separator (HS) is a dielectric mirror that transmits 1064 nm wavelength and has a high reflectivity for 532 nm, whereas DM is a 1000 nm-cutoff wavelength dichroic mirror. The microwave field generated during the magnetization precession is detected by means of an antenna critically coupled to the TE_{102} mode and connected through a short transmission line to a 39 dB-gain amplification stage A. The amplified signal is finally registered at a 20 GHz sampling oscilloscope.

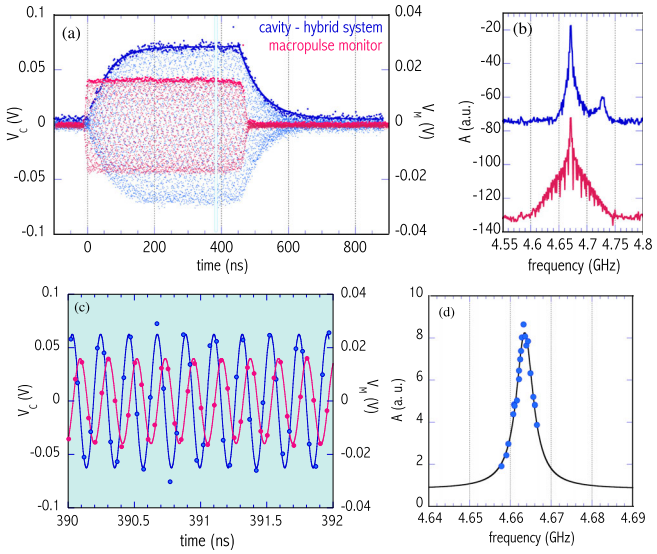

FIG. 3. Optically driven spin precession in the time and frequency domain. (a) Oscilloscope traces displaying both the amplified signal V_C detected in the microwave cavity hosting the YIG sphere (blue) and the output V_M of the laser macropulse monitor (red). (b) Fourier transform amplitude spectrum of the microwave signals displayed in (a). The logarithmic scale is used for the vertical axis. (c) 2 ns-duration zoom out of (a) showing the magnetization precessing synchronously with the laser pulses. (d) Tuning the laser repetition rate to the hybridized frequency f_-.

illustrated in Fig. 2 is used to investigate the optomagnetic phenomenon. The 7.2 ps-duration, 1.55 μm-wavelength laser pulses are obtained at the idler output of an OPO, synchronously pumped by the second harmonic of a master oscillator power amplifier (MOPA) laser system that has been described elsewhere [24]. It is important to note that we are exploiting a nonabsorptive mechanism as the optical wavelength is within the YIG transparency window (1.5–5 μm). The beam waist at the YIG position is 1.28 mm, and the average intensity of the incident pulses is 2.4 $\mathrm{MW/cm^2}$, obtained within $< 1\,\mu$s-duration macropulses.

In Fig. 3 we demonstrate the all-optical coherent control of the magnon-photon mode at $f_- = 4.67$ GHz by employing a train of laser pulses with repetition rate f_r tuned to f_-. The rise and decay time of the microwave pulse registered at the oscilloscope agrees with the mode decay time $\bar{\tau} = 65$ ns we get through the S^{21} measurements within experimental errors. The duration of the optical excitation is set to a value of $t_e \simeq 0.5\ \mu\mathrm{s} > \bar{\tau}$ allowing us to control the system in its steady state. This differs from previous studies in optomagnetism that were focused on the transient optical control of the magnetization via single femtosecond laser pulses (see [1], and references therein).

Moreover, the YIG magnetization precesses in phase with the laser pulses, as demonstrated by juxtaposition in Fig. 3(c) of the signal generated in the microwave cavity and the output of the laser macropulse monitor WM, i.e., a coaxial waveguide hosting a nonlinear crystal in which microwaves are generated through optical rectification [23]. Another important signature of the coherent precession of the magnetization is also shown in Fig. 3(d), where the amplitude of the Fourier transform of the microwave signal is plotted for different values of the laser repetition rate f_r. The data are fitted to a Lorentzian curve that takes into account the convolution between the optical excitation and the profile of the hybridized mode at 4.6711 GHz. As shown in Fig. 3(b), the spectral component f_+ is also excited but with a much smaller strength. These results, combined with the assessment of stationary precession of the macroscopic magnetization, unambiguously show that each macropulse acts as an effective microwave field on the ensemble of strongly correlated spins of the FMR mode.

Discussion.—To confirm the nonthermal origin of the laser-induced magnetization precession we investigated the dependence of the microwave signal amplitude on the laser polarization [1] and the results are reported in Fig. 4(a). A linearly polarized pulse induces an effective magnetic field that depends on the relative orientation of the polarization

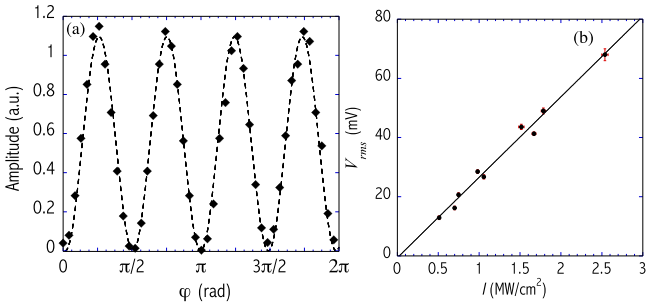

FIG. 4. (a) Amplitude of the microwave signal in the cavity as a function of the laser polarization angle. (b) Magnetization dependence on the laser intensity.

vector and the YIG crystallographic axes. This field tilts the magnetization vector away from the $\mathbf{B}_{\text{ext}}$ direction, and a sequence of pulses can coherently excite magnetization oscillations if their repetition rate is tuned to the FMR resonance. Actually the observed magnetization precession is induced by a second-order process conveniently described by a third-rank, axial time-odd tensor $\chi^{(2)}_{ijk}$, provided that $\mathbf{k}$ is orthogonal to the [110] crystal direction $\mathbf{d}$ [8]. As the reference system axes x and y coincide with $\mathbf{k}$ and $\mathbf{d}$ directions, the photoinduced magnetization lies in the yz plane and reads

$$M_i = \int d\Omega \chi^{(2)}_{ijk} E^{\star}_j(\Omega) E_k(\Omega), \tag{3}$$

where $i = 2,\ 3$, and $E_2(\Omega) = E(\Omega)\cos\varphi$ and $E_3(\Omega) = E(\Omega)\sin\varphi$; here $E(\Omega)$ is the Fourier transform of the laser electric field oscillating at ~190 THz and φ is the polarization angle of the incident light with respect to the y axis. The susceptibility $\chi^{(2)}_{ijk}$ and magnetization have only the 0 and 2Ω components. On the other hand, in the adiabatic condition $\omega \ll \Omega$ the down-converted zero frequency magnetization can be replaced by a slowly varying $M_i(\omega)$. Because of well-known symmetries of second-order susceptibility [1], the nonvanishing components of χ_{ijk} are $\chi_{233} = -\chi_{222} = \chi_{332} = \chi_{323} \equiv \Xi(\omega)$ and Eq. (3) gives the components

$$M_z = \int d\omega \Xi(\omega) |E(\omega)|^2 \cos 2\varphi, \tag{4}$$

$$M_y = \int d\omega \Xi(\omega) |E(\omega)|^2 \sin 2\varphi. \tag{5}$$

Note that only the oscillating z component of the magnetization gives rise to the detected microwave field. Around the hybridized mode frequencies $\omega_{\pm}$, the real and imaginary part of the complex susceptibility $\Xi(\omega)$ can be approximated by absorption $\Xi(\omega)''$ and dispersion $\Xi(\omega)'$ components of magnetization [25]. In particular, at working frequency ω_- we have only absorption with no dispersion; hence, the susceptivity $\Xi(\omega_-) = \Xi_0 \omega_- \bar{\tau}/2$ becomes real, and does not affect the magnetization direction. Thus the fulfillment of the resonant condition also allows us to simplify the geometric description of the photoinduced magnetization vector. Indeed, to explain the fourfold periodicity of the plot displayed in Fig. 4 (a) we only need to realize that the cavity selects the $M_z \propto \cos 2\varphi$ component via its geometric projection on the TE_{102} mode (i.e., the z direction as shown in Fig. 1), and that the critically coupled antenna cannot distinguish between parallel and antiparallel orientation of M_z. Therefore the detected magnetization signal must be proportional to $|\cos 2\varphi|$, as confirmed by the fit to the data in Fig. 4(a). Figure 4(b) shows instead the linearity of the measured spin oscillation amplitude as a function of the pump laser intensity, in agreement with Eq. (3) as well.

The strength of the effective microwave field B_{eff} that drives the M_z precession can be estimated thanks to the peculiar dynamics of hybridization. In general, the absorbed power in stationary conditions by a magnetized sample [25] is given by

$$P_a = V_s \left\langle -\mathbf{B} \cdot \frac{d\mathbf{M}}{dt} \right\rangle,$$

where $\langle\cdot\rangle$ denotes the time average over one period and V_s is the volume of the sample. Moreover, at resonance and for a critically coupled inductive loop, the measured power in the microwave cavity is $P_a/2$. In our experimental conditions, the absorbed power by the YIG crystal at the frequency ω_-

$$P_a = V_s \Xi_0 \omega_-^2 \bar{\tau} \frac{B^2_{\text{eff}}}{\mu_0} \tag{6}$$

is written in terms of quantities that are measured or fitted to the data, so that the second-order susceptivity can be readily estimated through $\Xi_0 = P_a \mu_0/(V_s \omega_-^2 \bar{\tau} B^2_{\text{eff}})$, where B_{eff} represents the laser-induced effective magnetic field. Because of $1/f$ dependence of the power spectrum generated by down conversion of the picosecond frequency comb, the infrared optical field average amplitude $B_l = \sqrt{\mu_0 I/c} = 10$ mT, at $f_o \simeq 190$ THz optical frequency, is suppressed to $B_{\text{eff}} = 2.5 \times 10^{-5} B_I = 0.25\ \mu$T at $f_- \sim 4.7$ GHz. With $P_a = 3$ nW estimated from the plots reported in Fig. 3, we eventually get $\Xi_0 \sim 10^{-7}$ cm^2/MW.

In summary, our experimental and theoretical approach provides a purely optical, flexible technique to manipulate the magnetization vector in YIG via polarization rotation and intensity modulation of the incident laser beam. Remarkably, in free space the maximum control speed of the magnetization through the described resonant excitation is only limited by the linewidth of the selected resonance. It is worth mentioning that commercially available compact ultrafast cw oscillators with 200 pJ-energy output pulses [26] may foster applications of the present method in the optomagnetism field.

Unlike the ingenious optical method described in Ref. [8], here the mode-locked pulses impinging on the magnetized material allow for operation of the system in the steady state, opening a path on the ultrafast laser control of hybridized magnon-photon systems.

The authors thank D. Budker and V. S. Zapasskii for carefully reading the manuscript and useful discussions. C. B. and M. G. acknowledge partial financial support of the University of Padova under Progetto di Ateneo (Grant No. CPDA135499/13). Technical support by E. Berto is gratefully acknowledged.

*caterina.braggio@unipd.it
†antonello.ortolan@lnl.infn.it

[1] A. Kirilyuk, A. V. Kimel, and T. Rasing, Rev. Mod. Phys. **82**, 2731 (2010).
[2] C. D. Stanciu, F. Hansteen, A. V. Kimel, A. Kirilyuk, A. Tsukamoto, A. Itoh, and T. Rasing, Phys. Rev. Lett. **99**, 047601 (2007).
[3] T. Li, A. Patz, L. Mouchliadis, J. Yan, T. A. Lograsso, I. E. Perakis, and J. Wang, Nature (London) **496**, 69 (2013).
[4] Z.-L. Xiang, S. Ashhab, J. Q. You, and F. Nori, Rev. Mod. Phys. **85**, 623 (2013).
[5] D. Zhang, X.-M. Wang, T.-F. Li, X.-Q. Luo, W. Wu, F. Nori, and J. You, npj Quantum Info. **1**, 15014 (2015).
[6] A. V. Kimel, A. Kirilyuk, P. A. Usachev, R. V. Pisarev, A. M. Balbashov, and T. Rasing, Nature (London) **435**, 655 (2005).
[7] A. M. Kalashnikova, A. V. Kimel, R. V. Pisarev, V. N. Gridnev, P. A. Usachev, A. Kirilyuk, and T. Rasing, Phys. Rev. B **78**, 104301 (2008).
[8] N. Kanda, T. Higuchi, H. Shimizu, K. Konishi, K. Yoshioka, and M. Kuwata-Gonokami, Nat. Commun. **2**, 362 (2011).
[9] U. Keller, Nature (London) **424**, 831 (2003).
[10] S. T. Cundiff and J. Ye, Rev. Mod. Phys. **75**, 325 (2003).
[11] C. Kittel, *Introduction to Solid State Physics*, 8th ed., edited by S. Vonsovskii (John Wiley & Sons, New York, 2005).
[12] F. Hansteen, A. Kimel, A. Kirilyuk, and T. Rasing, Phys. Rev. Lett. **95**, 047402 (2005).
[13] T. Satoh, Y. Terui, R. Moriya, B. A. Ivanov, K. Ando, E. Saitoh, T. Shimura, and K. Kuroda, Nat. Photonics **6**, 662 (2012).
[14] A. A. Serga, A. V. Chumak, and B. Hillebrands, J. Phys. D **43**, 264002 (2010).
[15] Y. Kajiwara, K. Harii, S. Takahashi, J. Ohe, K. Uchida, M. Mizuguchi, H. Umezawa, H. Kawai, K. Ando, K. Takanashi, S. Maekawa, and E. Saitoh, Nature (London) **464**, 262 (2010).
[16] D. Bossini, S. Dal Conte, Y. Hashimoto, A. Secchi, R. V. Pisarev, T. Rasing, G. Cerullo, and A. V. Kimel, Nat. Commun. **7**, 10645 (2016).
[17] N. Bloembergen and R. V. Pound, Phys. Rev. **95**, 8 (1954).
[18] M. O. Scully and M. S. Zubairy, *Quantum Optics* (Cambridge University Press, Cambridge, 1997).
[19] H. Huebl, C. W. Zollitsch, J. Lotze, F. Hocke, M. Greifenstein, A. Marx, R. Gross, and S. T. B. Goennenwein, Phys. Rev. Lett. **111**, 127003 (2013).
[20] X. Zhang, C.-L. Zou, L. Jiang, and H. X. Tang, Phys. Rev. Lett. **113**, 156401 (2014).
[21] Y. Tabuchi, S. Ishino, T. Ishikawa, R. Yamazaki, K. Usami, and Y. Nakamura, Phys. Rev. Lett. **113**, 083603 (2014).
[22] L. Bai, M. Harder, Y. P. Chen, X. Fan, J. Q. Xiao, and C. M. Hu, Phys. Rev. Lett. **114**, 227201 (2015).
[23] C. Braggio and A. F. Borghesani, Rev. Sci. Instrum. **85**, 023105 (2014).
[24] A. Agnesi, C. Braggio, L. Carrà, F. Pirzio, S. Lodo, G. Messineo, D. Scarpa, A. Tomaselli, G. Reali, and C. Vacchi, Opt. Express **16**, 15811 (2008).
[25] F. Fiorillo, *Characterization and Measurement of Magnetic Materials* (Elsevier, New York, 2004).
[26] L. Krainer, R. Paschotta, S. Lecomte, M. Moser, K. Weingarten, and U. Keller, IEEE J. Quantum Electron. **38**, 1331 (2002).